

Computational Investigation of 2-D Temperature Distribution in Static Liquid Metals Exposed to Steady State Plasmas^{*)}

Nopparit SOMBOONKITTICHAJ

Department of Physics, Faculty of Science, Kasetsart University, Chatuchak, Bangkok 10900, Thailand

(Received 10 January 2022 / Accepted 24 April 2022)

Understanding the temperature distribution in a liquid metal under plasma bombardment is required for characterizing and controlling their own impurity releases and heat transfer. To achieve this, a 2-D heat conduction inside a static liquid bombarded by a plasma is numerically solved in this study. Thin layers consist of Al, Li, In, Sn and Ga. Plasma constituents are D and Ar. The liquid temperature is initialized by melting temperature. The upper surface is heated by ions and electrons but cooled by evaporation and thermal radiation. The lower surface is in contact with the boundary conditions: the fixed melting temperature for characterizing the temperature spread influenced by different thermal diffusivities and ion masses; and the floating temperature governed by convective cooling and thermal radiation for characterizing the heat transfer across the liquid provided by the implementation of a coolant. It appears that Al conducts heat well so the temperature distribution is smoothed out, probably a choice for excessive heat flushing during abnormal events. Sn and In may be good undesirable impurity collectors because of low evaporation with less coolant concern, but not for Li and Ga.

© 2022 The Japan Society of Plasma Science and Nuclear Fusion Research

Keywords: plasma facing component, plasma surface interaction, liquid metal, Maxwell-Boltzmann distribution, floating potential, heat conduction, thermal radiation, convective cooling, Hertz-Knudsen-Langmuir (HKL) equation, Forward Time Central Space (FTCS) difference

DOI: 10.1585/pfr.17.2405073

1. Introduction

In recent years, low melting and/or low-Z metal liquid layers have been tested in several fusion tokamak operations as plasma facing components, controlled by specific designed circulation devices. This can be exemplified by lithium (Li) implementations in T-11 M [1, 2], HT-7, and EAST [1,3] and gallium (Ga) implementations in T-3 M [2] and ISTTOK [4].

The installation of liquid metals as plasma facing components are generally to

1. reduce and prevent re-injection of recycling hydrogen species and other wall accumulated impurities due to the ability of a liquid to be made flowing after allowing impurities being absorbed, so that they can be flushed away from a main chamber,
2. improve the operational time period, especially the case that the liquid species is compatible with hydrogen isotopes, e.g. low-Z species, and
3. provide the opportunity for a damaged surface to access self-repairing caused by intense heat load deposition.

The study on this issue is still currently very active because of its benefits and also its disadvantage, at which the installation is not optimized to achieve the balance among plasma profiles, an installation site, a liquid layer tempera-

ture, a structural configuration and a coolant design. This is to remedy the production of the unwanted impurities provided by the liquid itself. The evidence of the disruption observation caused by a large quantities of liquid impurity releases by heavy heat load at which the liquid layer is near a core plasma has been reported in [3].

It must be noted that the compatibility with the plasma species and the activation of liquid substances under fusion environments are not the main concerns in this study, because the study is concentrated on understanding the physics of thermal transport in the selected liquid pure metals, i.e. aluminum (Al), lithium (Li), indium (In), tin (Sn) and gallium (Ga), under plasma surface interactions provided by the selected plasmas, i.e. deuterium (D) and argon (Ar).

However, it may be useful to discuss on their availability and activation, and the time for them decaying to be low level waste (LLW) prior to considering the detail of this study. As reported in [5], Li and Ga are attractive in terms of low neutron activation, in opposition to Al and In, providing large neutron activation and being limited in usage based on radioactive safety. In addition, 10% usage of Sn is possible in a nuclear reactor because of moderate neutron activation [5]. The report [5] also suggests that Al is naturally abundance, but the rest will be short of their reserves in a few hundreds years, especially Ga and In. With regards to the time required for being LLW [6], Ga, In and Al are good candidates because the time for them

author's e-mail: fscinrso@ku.ac.th

^{*)} This article is based on the presentation at the 30th International Toki Conference on Plasma and Fusion Research (ITC30).

being LLW is less than 200 years. In spite of this, Li and Sn just need a slightly longer time, i.e. only a few hundreds years more, to decay to LLW. This implies that their overall potentials to be liquid surfaces in future nuclear fusion reactors are still debatable. Thus, other criteria, e.g. heat transfer under plasma bombardment, should be investigated. This inspires conducting this study.

The main scope is to be focused on the heat transfer under plasma surface interactions between steady state plasmas and static liquid pure metals. A temperature distribution inside a static liquid layer is revealed by the two dimension transient heat conduction equation. The Maxwell-Boltzmann distribution, which is a good approximation for describing a steady state plasma faraway from a plasma exposed surface approximately 10 times of Debye length from the surface (see figure 2.6 in [7]), are mainly exploited to derive particle, momentum and energy fluxes, together with some assumptions, at a surface. Such fluxes usually dictate plasma surface interactions, thereafter, affect the inner liquid temperature distribution. Firstly, a floating potential on a plasma charged surface, known to be a summative parameter to essentially manipulate plasma surface interactions, is required to be determined through the equilibrium of one-way ion and electron fluxes on the surface. Subsequently, it involves in the derivations of an ion pressure, an electron pressure, and an electrostatic pressure, a pressure due to evaporation, and consequently a net pressure on the liquid surface. This will be outlined in section 2, especially sections 2.1 and 2.2. The floating potential is also associated with the estimation of ion and electron heat fluxes. Apart from this, the cooling fluxes on the plasma exposed surface consisting of thermal radiation and surface evaporation are introduced. These will be outlined in section 2.3. The solver, consisting of the discretized form of the heat conduction equation, and two types of boundary conditions are outlined in sections 2.4 and 2.5. This is unlike the study of [8], which implemented the lumped heat capacity approach [9] to study the liquid temperature. The selected liquid metallic substances, plasma constituents and parameters, and other parameters are mentioned in sections 2.6 and 2.7. Additional assumptions are adopted as follows, a pressure due to sputtering and a neutral pressure at the plasma exposed liquid surfaces are neglected, and the plasmas are fully ionized and unmagnetized. Section 3 provides the results and discussions on the effects of thermal diffusivity, plasma ion mass and the implementation of a coolant to the temperature distribution inside a charged liquid layer. Even though, a natural convection is not fully considered in this study, the difference between the results being outcome from the heat conduction alone and that modified by the natural convection is briefly discussed before a conclusion in section 4.

2. Methodology

Incoming ions and electrons are assumed to be not

reflected back to the plasma after hitting the liquid surface. In addition, the relatively negative potential on the surface is usually preset by plasma electron bombardment in very short timescale described by the inverse of plasma frequency. Subsequently, all ions, but only high energy electrons, reach the surface. Plasma ion flux (Γ_i) arriving at the charged surface is estimated by the multiplication of ion density (n_i) and ion sound speed (c_s), $\Gamma_i = n_i c_s = n_i \sqrt{\frac{k_B T_e + \gamma k_B T_i}{m_i}}$ [7], as follows

$$\Gamma_i = n_i \sqrt{\frac{e T_e [eV]}{m_i}} (1 + \gamma \beta), \quad (1)$$

where $T_e [eV]$ ($= \frac{k_B T_e}{e}$) is an electron temperature in eV unit, e is an elementary charge, m_i is a single ion mass, k_B is the Boltzmann constant, γ is the specific heat capacity ratio ($\gamma = \frac{5}{3}$ is used by assuming that the plasma is under the adiabatic process) and β ($= \frac{T_i}{T_e}$) is the ratio of ion to electron temperatures, and plasma electron flux (Γ_e) is determined through the one-way Maxwellian flux [7] as

$$\begin{aligned} \Gamma_e &= \int_{-\infty}^{\infty} \int_{-\infty}^{\infty} \int_{v_{e,\perp}=0}^{\infty} v_{e,\perp} f_e^{M-B}(v_e) d^3 \mathbf{v}_e, \\ &= \frac{1}{4} n_e \exp\left(\frac{e \phi_f}{k_B T_e}\right) \sqrt{\frac{8 k_B T_e}{\pi m_e}}, \\ &= \frac{1}{4} n_e \exp\left(\frac{\phi_f}{T_e [eV]}\right) \sqrt{\frac{8 e T_e [eV]}{\pi m_e}}, \end{aligned} \quad (2)$$

where n_e is an electron density, m_e is a single electron mass, $v_{e,\perp}$ is an electron speed perpendicular to a surface, and $f_e^{M-B}(v_e) = n_e \left(\frac{m_e}{2\pi k_B T_e}\right)^{3/2} \exp\left(-\frac{\frac{1}{2} m_e v_e^2 - e \phi_f}{k_B T_e}\right)$ is the Maxwell-Boltzmann distribution of plasma electrons under the presence of an electric field (\mathbf{E}) due to a potential difference. The floating potential (ϕ_f), which is the potential difference between the bulk plasma and its exposed surface, is determined at equilibrium by $\frac{d(e \Gamma_i - e \Gamma_e)}{dt} = 0 \Rightarrow \Gamma_i = \Gamma_e$ [7]. This leads to

$$\phi_f = 0.5 T_e [eV] \ln\left(2\pi \frac{m_e}{m_i} (1 + \gamma \beta)\right). \quad (3)$$

2.1 Ion and electron pressures

Ion (P_i) and electron (P_e) pressures on a planar surface during plasma bombardment need to be determined because they crucially involve in other processes on the surface, i.e. an evaporation rate and a net pressure in this study. The work of [8] previously provided only their expressions without illustrating their derivations. Hence, the derivations are illustrated here. Under the assumption that a plasma is collisionless, P_i and P_e with their derivations using the Maxwellian moment [7] are going to be provided as follows,

$$\begin{aligned} P_i &= \int_{-\infty}^{\infty} \int_{-\infty}^{\infty} \int_{v_{i,\perp}=0}^{\infty} (m_i v_{i,\perp, s}) v_{i,\perp} f_i^{M-B}(v_i) d^3 \mathbf{v}_i, \\ &= m_i n_i \sqrt{\frac{m_i}{2\pi k_B T_i}} \int_0^{\infty} v_{i,\perp} \sqrt{v_{i,\perp}^2 + \frac{2e|\phi_f|}{m_i}} \end{aligned}$$

$$\begin{aligned}
 & \times \exp\left(-\frac{m_i v_{i,\perp}^2}{2k_B T_i}\right) dv_{i,\perp}, \\
 & = 0.5n_i k_B T_i \left(\exp\left(\frac{e|\phi_f|}{k_B T_i}\right) \left(1 - \operatorname{erf}\left(\sqrt{\frac{e|\phi_f|}{k_B T_i}}\right)\right) \right. \\
 & \quad \left. + \frac{2}{\sqrt{\pi}} \sqrt{\frac{e|\phi_f|}{k_B T_i}} \right), \\
 & = 0.5n_i e \beta T_e [eV] \\
 & \quad \times \left(\exp\left(\frac{\Phi_f}{\beta}\right) \operatorname{erfc}\left(\sqrt{\frac{\Phi_f}{\beta}}\right) + 2\sqrt{\frac{\Phi_f}{\pi\beta}} \right), \quad (4)
 \end{aligned}$$

where $v_{i,\perp,s} = \sqrt{v_{i,\perp}^2 + \frac{2e|\phi_f|}{m_i}}$ and $v_{i,\perp}$ are ion speeds, perpendicular to the surface, at the surface and in the bulk plasma, where the electrostatic potential is set up to be zero as a reference, in turn and $\Phi_f = \frac{|\phi_f|}{T_e [eV]}$, and

$$\begin{aligned}
 P_e & = \int_{-\infty}^{\infty} \int_{-\infty}^{\infty} \int_{v_{e,\perp}=0}^{\infty} (m_e v_{e,\perp}) v_{e,\perp} f_e^{M-B}(v_e) d^3 \mathbf{v}_e, \\
 & = n_e \left(\frac{m_e}{2\pi k_B T_e} \right)^{3/2} \int_{-\infty}^{\infty} (m_e v_{e,\perp}) v_{e,\perp} \\
 & \quad \times \exp\left(-\frac{\frac{1}{2}m_e v_e^2 + e|\phi_f|}{k_B T_e}\right) d^3 \mathbf{v}_e, \\
 & = 0.5n_e k_B T_e \exp\left(-\frac{e|\phi_f|}{k_B T_e}\right), \\
 & = 0.5n_e e T_e [eV] \exp(-\Phi_f). \quad (5)
 \end{aligned}$$

The exponential term is contributed from the electric field described by ϕ_f , as same as that of Γ_e . With regards to ions, the bulk plasma ions obey the general Maxwell-Boltzmann distribution, i.e. $f_i^{M-B}(v_i) = n_i \left(\frac{m_i}{2\pi k_B T_i}\right)^{3/2} \exp\left(-\frac{\frac{1}{2}m_i v_i^2}{k_B T_i}\right)$. In addition, the conservation of energy is adopted. This has to be noted that the expressions of P_i and P_e are valid only if the planar surface is relatively negative and no backscattering is assumed at a liquid surface.

2.2 Net surface pressure

A net pressure (P_{net}) on the charged planar surface, which also represents the liquid pressure at the surface at equilibrium, is as follows [8],

$$P_{net} = P_i + P_e - P_{es} + P_{evap}, \quad (6)$$

where $P_{es} = 0.5\epsilon_0 |\mathbf{E}|^2 = \frac{0.5\epsilon_0 \phi_f^2}{(10\lambda_D)^2}$ is an electrostatic pressure, [8], $P_{evap} = M\Gamma_{evap} \sqrt{\frac{8k_B T}{\pi M}}$ is a pressure due to evaporation [8], $\Gamma_{evap} = \frac{P_{net}}{\sqrt{2\pi M k_B T}}$ is an evaporation rate, named as the Hertz-Knudsen-Langmuir (HKL) equation [10]. ϵ_0 , λ_D , T and M are the vacuum permittivity, the electron Debye length, and the temperature and the mass of a single vaporized particle, respectively.

2.3 Net energy fluxes

A net energy flux (Ξ_{net}) results from ion (Ξ_i) [7] and electron (Ξ_e) [7] energy fluxes, thermal radiation flux

(Ξ_{rad}) [9] and evaporation cooling flux (Ξ_{evap}) [8], i.e. $\Xi_{net} = \Xi_i + \Xi_e - \Xi_{rad} - \Xi_{evap}$. Each following expression refers to each mentioned kind of the energy fluxes during the surface being exposed to the plasma as listed,

$$\Xi_i = (2\beta T_e [eV] + |\phi_f|) e \Gamma_i, \quad (7)$$

$$\Xi_e = 2e T_e [eV] \Gamma_e, \quad (8)$$

$$\Xi_{rad} = \sigma (T_{surf}^4 - T_{env}^4), \quad (9)$$

$$\Xi_{evap} = (2k_B T_{surf} + L) \Gamma_{evap}, \quad (10)$$

where T_{surf} is a liquid surface temperature, T_{env} is an environment temperature, L is a surface binding energy (or a latent heat) per particle and σ is the Stefan-Boltzmann constant. If a coolant is presented, then its convective cooling flux (Ξ_{conv}) described by the Newton's law of cooling [9] is

$$\Xi_{conv} = h(T_{surf} - T_{env}), \quad (11)$$

where h is a convective cooling coefficient.

2.4 Numerical solver for heat transfer

Several reasons supporting the aim in studying the temperature distribution inside the static liquid layer undergoing plasma surface interactions are:

1. various liquid substances have various thermal diffusivities, so that the trends of temperature spread inside the liquid layer become different;
2. various plasma species differently contribute the magnitude of net heating flux on a liquid surface; and
3. the trends of temperature spread inside the liquid layers behave even more differently if external coolants are imposed underneath the liquid layers.

The two dimension transient heat conduction equation with appropriate boundary conditions is exploited to study the temperature distribution in the charged static liquid layer in this work. In the bulk static liquid, its initial temperature is its melting temperature (T_{melt}). The heat conduction equation and its standard discretized form, obeying the Forward Time Central Space (FTCS) difference approach [9, 11, 12], are described by

$$\frac{1}{D} \frac{\partial T}{\partial t} = \frac{\partial^2 T}{\partial x^2} + \frac{\partial^2 T}{\partial y^2}, \quad (12)$$

$$\begin{aligned}
 T_{i,j}^{k+1} & = S (T_{i+1,j}^k + T_{i,j+1}^k + T_{i-1,j}^k + T_{i,j-1}^k) \\
 & \quad + (1 - 4S) T_{i,j}^k, \quad (13)
 \end{aligned}$$

where T is a liquid temperature, $D = \left(\frac{k}{\rho c_p}\right)$ is a thermal diffusivity, $\partial t \rightarrow \delta t$, $\partial x = \partial y \rightarrow \delta s$, $S = \frac{D\delta t}{(\delta s)^2}$, the i^{th} , j^{th} and k^{th} indexes are associated with the discrete directions of spatial y - and x -axes, and time (t), and k , ρ and c_p represent a thermal conductivity, a mass density and a constant-pressure specific heat capacity.

2.5 Boundary conditions

The fixed rectangular shape of a liquid layer is assumed. Only the upper boundary is faced towards a steady state plasma, which is characterized by n_i , n_e , T_i , T_e and m_i . The left and the right boundary conditions are a constant temperature at the melting temperature (T_{melt}) of each considered liquid material. This is reasonable because the inlet and the outlet of the liquid should be in contact with the heating device which maintains T_{melt} . The discretized boundary conditions in terms of the temperatures of the upper (T_U), the left (T_L) and the right (T_R) boundaries are

$$T_U^{k+1} = T_{M,j}^{k+1} = (1 - 2S)T_{M,j}^k + 2ST_{M-1,j}^k + \frac{2\Xi_{net}\delta t}{\rho c_p \delta s}, \quad (14)$$

where the M^{th} index represents the set of the grid points at the upper surface, and

$$T_L = T_R = T_{melt}. \quad (15)$$

For the lower boundary, it is characterized by two cases:

1. a fixed temperature boundary, corresponding to the existence of a heating device maintaining T_{melt} like T_L and T_R ,

$$T_B = T_{melt}. \quad (16)$$

2. a floating temperature boundary, corresponding to the existence of convective cooling and thermal radiation,

$$T_B^{k+1} = T_{0,j}^{k+1} = (1 - 2S)T_{0,j}^k + 2ST_{1,j}^k + \frac{2\Xi_{cool}\delta t}{\rho c_p \delta s}, \quad (17)$$

where the 0^{th} index represents the set of the grid points at the lower surface.

The net energy flux at the upper boundary becomes $\Xi_{net} = \Xi_j + \Xi_e - \Xi_{evap} - \Xi_{rad}$, where T_{env} is assumed to be 1500 K, while the net cooling flux at the lower boundary becomes $\Xi_{cool} = \Xi_{conv} + \Xi_{rad}$, where T_{env} of Ξ_{conv} and Ξ_{rad} are T_{melt} . The control volume method [9, 11] is applied for the boundary condition discretization.

2.6 Surface material properties

Al, Li, In, Sn and Ga are selected to be studied due to low T_{melt} . With regards to the thermal properties, the thermal diffusivities ($D = \frac{k}{\rho c_p}$) of Al, Li, In, Sn and Ga are 1.11×10^{-4} , 4.54×10^{-5} , 4.99×10^{-5} , 4.20×10^{-5} and 1.79×10^{-5} $\text{m}^2 \text{s}^{-1}$, where k , ρ and c_p are tabulated in Table 1. In fact, $D_{Ga} < D_{Li} (\approx D_{In} \approx D_{Sn}) < D_{Al}$. In addition, T_{melt} and T_{boil} (boiling temperatures), and the liquid temperature ranges (ΔT_{liq}) of Al, Li, In, Sn and Ga are tabulated in Table 2, which can be summarized that $\Delta T_{liq,Li} \ll \Delta T_{liq,Al} (\approx \Delta T_{liq,In}) < \Delta T_{liq,Ga} < \Delta T_{liq,Sn}$. The static liquid layer is assumed to be 10^{-3} m in thickness (ℓ).

Table 1 Material thermal properties [13].

Material	Al	Li	In	Sn	Ga
$c_p (\times 10^3)$ ($\text{J} \cdot \text{kg}^{-1} \cdot \text{K}^{-1}$)	0.897	3.582	0.233	0.227	0.373
$\rho (\times 10^3)$ ($\text{kg} \cdot \text{m}^{-3}$)	2.377	0.520	7.02	6.979	6.08
k ($\text{W} \cdot \text{m}^{-1} \cdot \text{K}^{-1}$)	237	84.7	81.6	66.6	40.6

Table 2 Melting (T_{melt}) and boiling (T_{boil}) temperatures [13] and calculated liquid temperature ranges (ΔT_{liq}).

Material	T_{melt} (K)	T_{boil} (K)	ΔT_{liq} (K)
Al	933.47	2792.5	1859.03
Li	453.65	1615.15	1161.5
In	429.75	2300.15	1870.4
Sn	505.08	2859.15	2354.07
Ga	302.9166	2502.15	2199.23

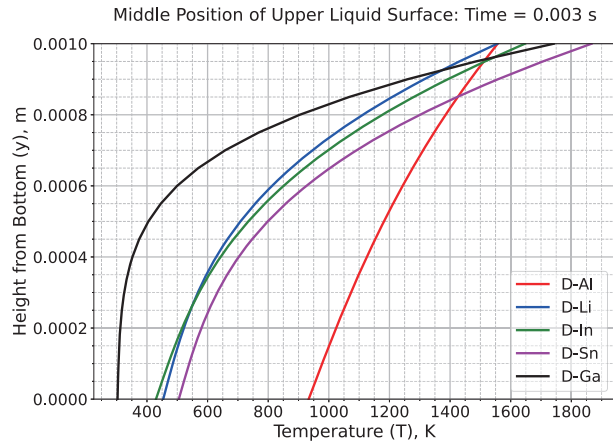
2.7 Plasma parameters and others

Plasma species are D and Ar, which represent small and large ion mass (m_i) in this study. Their $n_e = n_i = n = 10^{19} \text{ m}^{-3}$ (quasi-neutrality), $T_e = 250 \text{ eV}$, and $\beta = 1.0$.

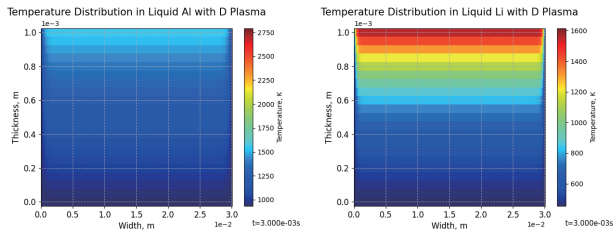
The selected convective cooling coefficients (h) are 0 (representing “no convective cooling”) and 40000 (representing “relatively large convective cooling”) $\text{W m}^{-2} \text{K}^{-1}$ without specifying the type of coolant used. (see Table 1 - 2 in [9]).

3. Result and Discussion

In this study, Al represents high D , Li, In and Sn represent moderate D , and Ga represents low D . To compare the trends of the temperature spread inside the liquid metals under the influence of various D , D plasma of $n = 10^{19} \text{ m}^{-3}$, $T_e = 250 \text{ eV}$, $\beta = 1.0$, and the fixed temperature boundary conditions are selected. Figure 1 (a) illustrates the temperature (T) distribution of each liquid substance from the plasma exposed (or upper) surface at its middle position. It is clearly seen that for low and moderate D , i.e. Ga, Li, In and Sn, high T is concentrated near their surface and their $\frac{\partial T}{\partial y}$ are relatively large from the surface into the liquid layer. Overall, $T - T_{melt} > 500 \text{ K}$ can be observed from approximately $0.7 \times 10^{-3} \text{ m}$ in height towards the surfaces at $t = 0.003 \text{ s}$ (see also Figs. 1 (b) - (f)). This implies that the deposited heat is not distributed well in the liquid Ga, Li, In and Sn layers. In contrast, if D is relatively high, i.e. Al, its $\frac{\partial T}{\partial y}$ is nearly constant. The deposited heat is well distributed into the volume of the liquid Al layer, justified through the trend of T . This implies that Al is good in efficiency in terms of spreading the deposited heat inside its volume under the same order of the net energy flux (Ξ_{net}) on the surface as that of Li, In, Sn and Ga (see the trends of Ξ_{net} of D and Ar plasmas in Fig. 2 (a)).

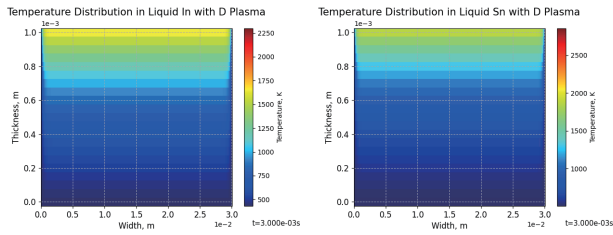


(a)



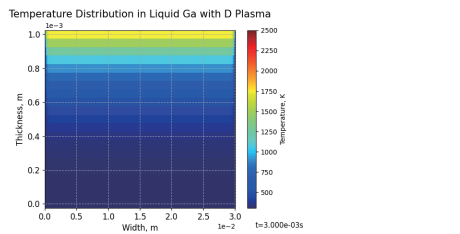
(b)

(c)



(d)

(e)

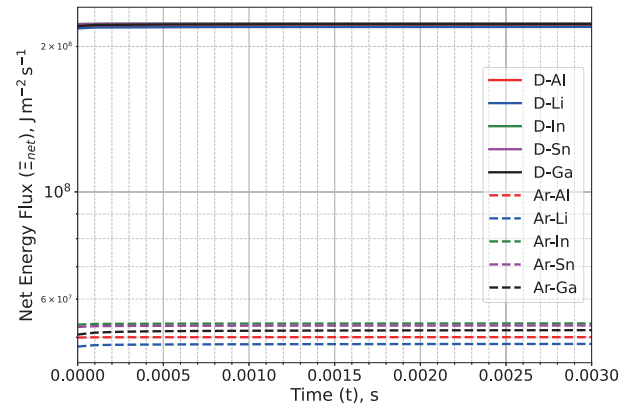


(f)

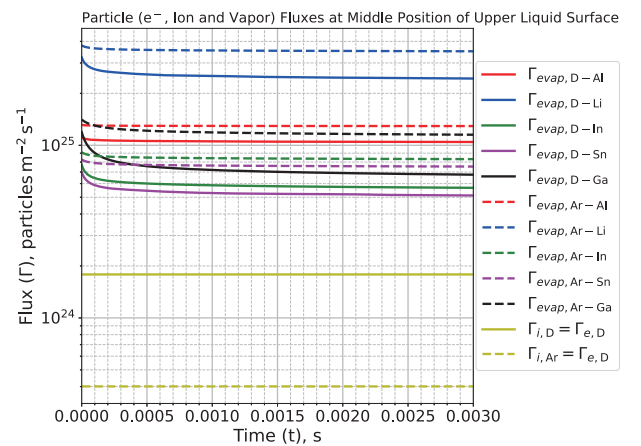
Fig. 1 (a) Temperature distributions at middle position of plasma exposed (or upper) surfaces of liquid Al, Li, In, Sn and Ga layers and (b)-(f) their 2-D temperature distributions, interacting with D plasma (color axis ranged from T_{melt} to T_{boil}), at the selected time ($t = 3$ ms).

In addition, it must be noted that with the same plasma parameters, the different ion mass (m_i) of a plasma plays an important role to govern both particle (Γ) and energy (Ξ) fluxes. $\Gamma_{i,D}$ ($= \Gamma_{e,D}$) on a charged liquid surface are greater than $\Gamma_{i,Ar}$ ($= \Gamma_{e,Ar}$), respectively (see the yellow thick and dash lines in Fig. 2 (b)). By this reason, $\Xi_{net,D}$ is greater than $\Xi_{net,Ar}$ (see Fig. 2 (a)). This is due to $m_{i,Ar} \gg m_{i,D}$, even though $|\phi_{f,Ar}| > |\phi_{f,D}|$. This means that a small m_i

Net Energy Flux at Middle Position of Upper Liquid Surface



(a)



(b)

Fig. 2 (a) Ξ_{net} , (b) Γ_i , Γ_e and Γ_{evap} at middle positions of liquid Al, Li, In, Sn and Ga upper surfaces by D and Ar plasmas.

plasma is great for surface heating. Apart from Ξ_{net} , Γ_{evap} , used to characterize the surface cooling and the depletion of a liquid volume during being exposed to a plasma, is also affected. With the current plasma parameters, P_{net} on the liquid Al, Li, In, Sn and Ga surfaces are of the same order, i.e. $P_{net} = 668 \pm 16$ and 784 ± 16 Pa for D and Ar plasmas in turn, but their Γ_{evap} are clearly different in terms of magnitude (see Fig. 2 (b)) because of the difference in the atomic masses (M) of the liquid substances. It appears that the liquid Li surface is heavily vaporized due to very small M . This implies that the concurrent Li replenishment is strongly required for a long-run plasma operation. In addition, a careful handling is also needed because a large quantities of the Li vapors surely contaminate the plasma. In contrast, the Sn and In liquids seem to be the good options for being the unwanted impurity collectors in the long-run plasma operation. This is because Sn and In provide the smallest and the second smallest Γ_{evap} , and additionally the largest and the third largest of ΔT_{liq} , so that being in liquid phase is longer in time period. Furthermore, T_{melt} of Sn and In are comparable to that of Li, so the

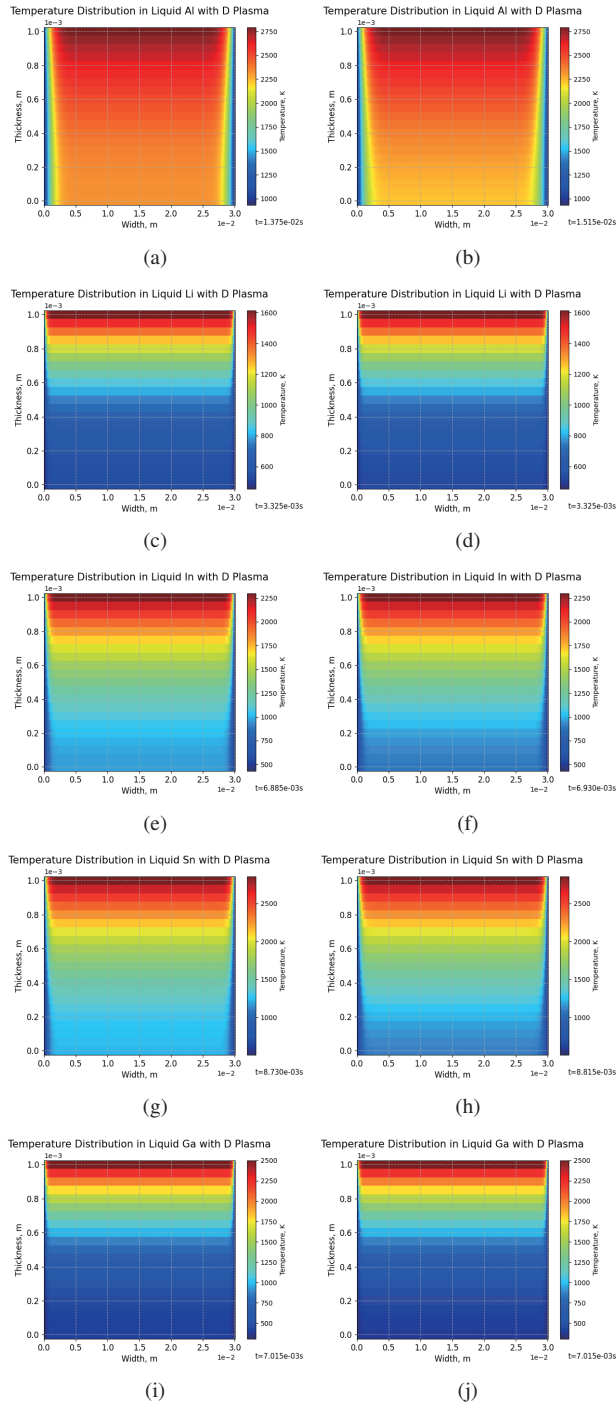


Fig. 3 2-D temperature distributions under ((a), (c), (e), (g) and (i)) thermal radiation ($h = 0 \text{ W m}^{-2} \text{ K}^{-1}$), and ((b), (d), (f), (h) and (j)) thermal radiation and convective cooling ($h = 40000 \text{ W m}^{-2} \text{ K}^{-1}$) of liquid Al, Li, In, Sn and Ga layers interacting with D plasma, where $T_{surf} = T_{boil}$, in turn.

they can be easily melted by a heating device of nearly the same specification. However, the higher neutron activation provided by In may be in concern of its usage.

The influence of a coolant, implemented beneath the liquid volume, to the temperature distribution can be investigated by adopting the floating temperature boundary.

Table 3 Elapsed times of $T_{surf} = T_{boil}$ for Al, Li, In, Sn and Ga surfaces under D and Ar plasmas.

Elapsed Time (ms) of $T_{surf} = T_{boil}$	$h = 0$ ($\text{W m}^{-2} \text{ K}^{-1}$)	$h = 40000$ ($\text{W m}^{-2} \text{ K}^{-1}$)
Al-D	13.752	15.157
Li-D	3.328	3.328
In-D	6.887	6.931
Sn-D	8.731	8.817
Ga-D	7.017	7.017
Al-Ar	70.1	$> 10^4$
Li-Ar	34.3	45.5
In-Ar	48.1	123.5
Sn-Ar	60.8	$> 10^4$
Ga-Ar	74.6	127.1

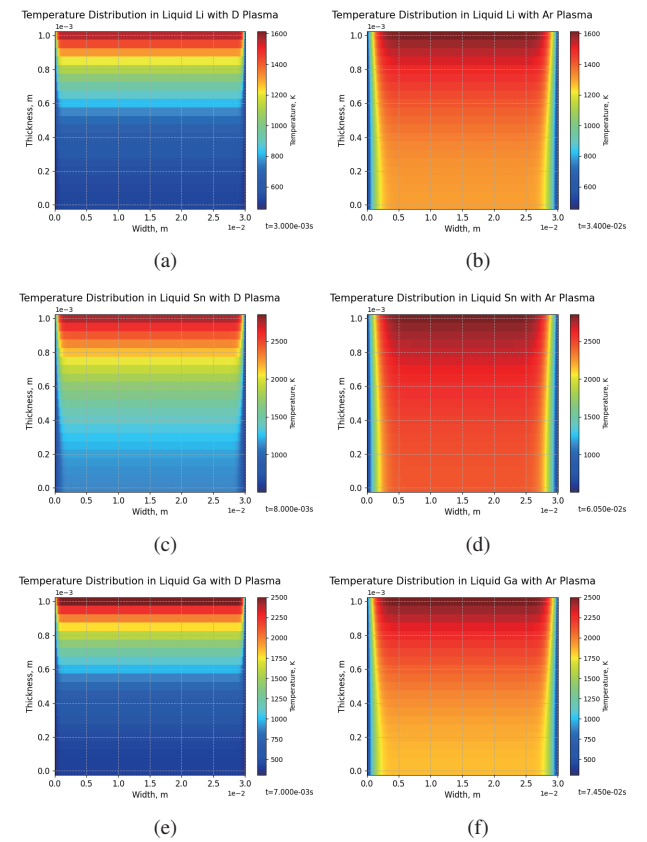


Fig. 4 2-D temperature distributions of liquid Li, Sn and Ga layers interacting with ((a), (c) and (e)) D and ((b), (d) and (f)) Ar plasmas, respectively, where $T_{surf} = T_{boil}$, under only thermal radiation ($h = 0 \text{ W m}^{-2} \text{ K}^{-1}$).

From this point, the lower boundary temperature can be varied by net cooling flux. With D plasma of $n = 10^{19} \text{ m}^{-3}$, $T_e = 250 \text{ eV}$, $\beta = 1.0$, Fig. 3 shows the 2-D temperature distributions of the liquid Al, Li, In, Sn and Ga layers of $\ell = 10^{-3} \text{ m}$, where $h = 0$ (only thermal radiation) and 40000 (strong convective cooling) $\text{W m}^{-2} \text{ K}^{-1}$ are taken into account. Overall, the coolant helps the temperature to be more spatially uniformly distributed in the vol-

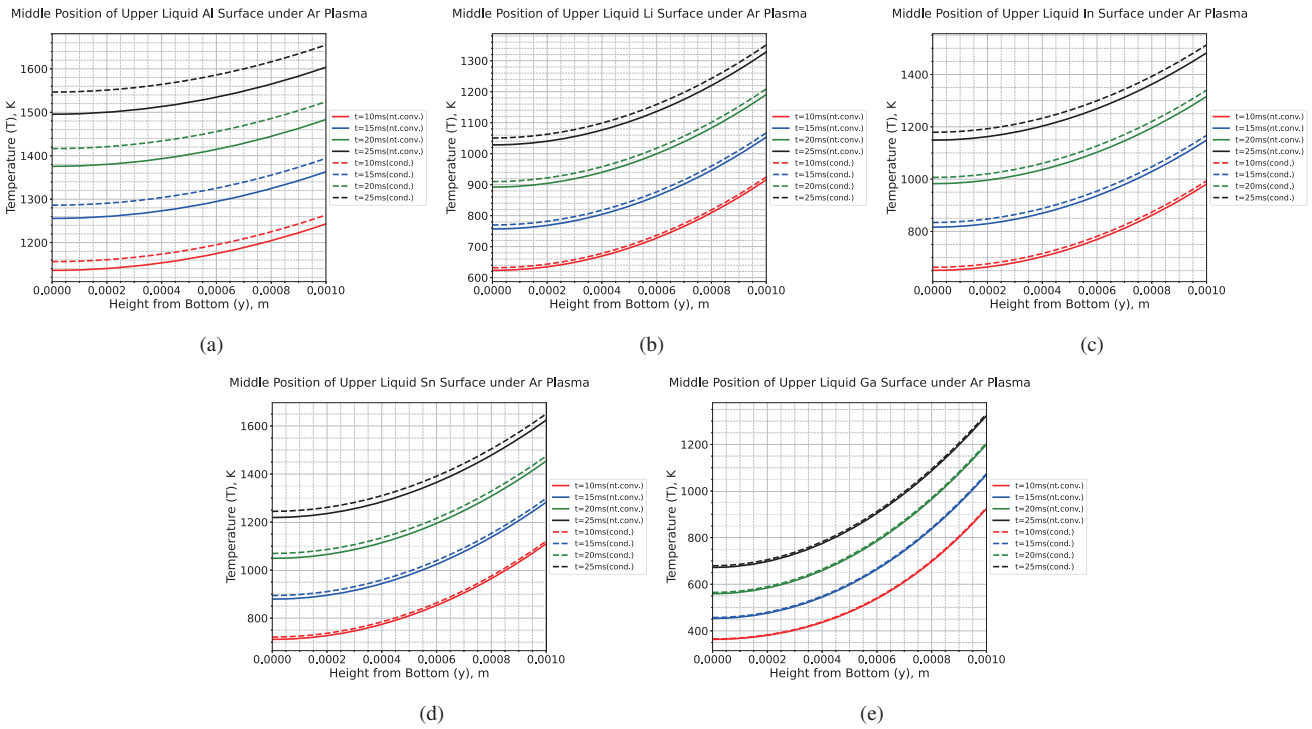


Fig. 5 Temperature distributions at middle positions of plasma exposed (or upper) surfaces of liquid (a) Al, (b) Li, (c) In, (d) Sn and (e) Ga layers under Ar plasma with and without implementing natural convection at the selected times: $t = 10, 15, 20$ and 25 ms.

ume. It extends the elapsed times before the surfaces reach T_{boil} . In fact, the coolant helps in prolonging the triggering of intense surface evaporation at T_{boil} , especially Al, In and Sn (see Figs. 3 (a) - (b) and (e) - (h), and Table 3). This is probably due to the good outcome of the combination of the relatively large D and ΔT_{liq} . This leads to good heat transfer in the volume together with well maintaining liquid phase. For Li and Ga, the elapsed time is not clearly seen to be extended. This should be because of the narrow ΔT_{liq} in case of Li and the low D in case of Ga, especially under D plasma. This suggests that the convective cooling of higher h compared with that used in this study, e.g. $h > 40000 \text{ W m}^{-2} \text{ K}^{-1}$, is essentially required if D and/or ΔT_{liq} of the liquid are small (see Figs. 3 (c) - (d) and (i) - (j), and Table 3).

If the Ar plasma with the same parameters is considered instead, the trends like above still correspond to those of D plasmas. However, the elapsed times of the liquid surfaces prior to $T_{surf} = T_{boil}$ are longer by approximately 5 to 20 times (see Fig. 4 and Table 3). This should be due to the fact that the smaller Ξ_{net} of Ar plasma is overwhelmingly balanced by Ξ_{cool} underneath the liquid layers. This smaller Ξ_{net} allows the inner temperature to have more time to thoroughly spread in the liquid layers. Furthermore, it is unexpectedly that the trends of T of the liquid Al and Sn layers under Ar plasmas approach to the nearly equilibrium, i.e. T at each inner position change very slow, where $T_{surf} < T_{boil}$ for very long time (see Table 3). The situation is seemingly maintained due to large D and/or ΔT_{liq} .

Even though, the methodology in this study is, until now, mainly relied on solely the heat conduction because a static fluid is assumed, it is undeniable that it is worth to ensure how much natural convection due to buoyancy, provided by the liquid density variation, should modify the prior results under this order of thickness, $\ell = 10^{-3}$ m. It must be noted that the detail of the study under the enhanced methodology including natural and other convections is going to published elsewhere [14], so only the brief comment on the natural convection affecting the prior trends of the inner temperature (T) of the Al, Li, In, Sn and Ga liquid layers under the D and Ar plasmas is stated here. An incompressible, inviscid and isotropic liquid with the Boussinesq approximation [11] are adopted to guide a natural convection. Only $h = 0 \text{ W m}^{-2} \text{ K}^{-1}$ is selected in order for one not to be confused with the effect of the convective cooling at the lower boundary in the T trends in the liquid layers. For all selected liquid materials under D plasma, the elapsed times for them to reach $T_{surf} = T_{boil}$ with and without including the natural convection do not clearly differ from one another. Probably, this is due to the situation that D plasma contributes large Ξ_{net} but thermal diffusivity (D) and an induced flow speed by natural convection, i.e. $u_{nv} \approx \sqrt{3\alpha g \ell \Delta T}$ [11] where α is a volumetric thermal expansion coefficient, g is the gravitational acceleration and $\Delta T = T - T_{rfc}$ (T_{rfc} is the reference temperature), are too low. This implies that the combination of D and ΔT_{liq} , together with the additional u_{nv} , insignificantly promotes the better T spread in Ξ_{net} and ℓ of these orders. In contrast to

the Ar plasma with the same parameters as D plasma, its lower Ξ_{net} causes less heat deposition rate on the liquid surfaces, so that with the combination of D , u_{nv} and ΔT_{liq} , the overall inner T of the Al, Li, In, Sn and Ga liquid layers are slightly decreased at the same time of consideration, i.e. $t = 10, 15, 20$ and 25 ms, by natural convection less than the order of 10%, e.g. approximately 7% for Al, 4% for In, Sn and Ga and 3% for Li (see the thick, representing “including natural convection” and the dash, representing “only heat conduction”, lines in Fig. 5).

4. Conclusion

As this study suggested, large atomic ion plasma, e.g. Ar, provides lower net heating flux than that of small ion mass plasma, e.g. D, so that the time for a liquid surface to reach its boiling temperature is longer. The coolant issue becomes less concerned. Also, the benefit provided by the combination of large thermal diffusivity and large liquid temperature range of a plasma exposed liquid surface plays a significant role for delaying its surface temperature reaching its boiling temperature. In some cases, e.g. liquid Al and Sn surfaces under Ar plasma, the surface temperatures are nearly in equilibrium and lower than the boiling temperatures. The use of a liquid metal surface in a fusion device, usually involving with hydrogen isotopes, requires very strong cooling. Selecting a liquid substance for being plasma facing components may need to correlate to the main objectives. Liquid aluminum may be a good choice for an excessive heat flushing, strictly used with a small quantity only at which an abnormal heat, e.g. during disruption and ELMs, normally bombards on because of high neutron activation. For capturing impurities and unfavorable species, liquid tin may be the better choice with the milder requirement of the cooling in contrast to liquid lithium, where the liquid temperature range is small, and liquid gallium, where thermal diffusivity is small in spite of large liquid temperature range comparable to that of liquid tin. In order to use liquid lithium and liquid gallium, which provide low activation, strong convective cooling are required. However, the usage of the liquid tin is precisely exploited only where the impurities and the unwanted species mostly shift to, because the safe usage have to be balanced with its moderate neutron activation. This implies why liquid indium may not be favorable in fusion. Finally, it needs to be commented that a natural convection in a static thin liquid metal layer clearly but slightly enhance in achieving

the well distributed inner temperature. The temperature of each inner position, to which the natural convection is applied, is not much smaller than that on which only heat conduction is concentrated. In fact, only a few percentages of difference are involved, but depends on layer thickness, net energy flux, thermal diffusivity, thermal expansion and liquid temperature range. Also, the inner temperature gradients do not clearly flatten.

Acknowledgements

N. Somboonkittichai deeply appreciates Dr. G. Z. Zuo (ASIPP, China) and Dr. J. Nakamura (JAEA, Japan) for good discussions on liquid metals, and S. Aiengkong and S. Somboonkittichai for encouragement. N. Somboonkittichai also thanks to the Python programming language [15] with the Numpy [16], Scipy [17] and Matplotlib [18] libraries for being available to be used in research without charge.

- [1] R.E. Nygren and F.L. Taberés, Nucl. Mater. Energy **9**, 6 (2016).
- [2] S.V. Mirnov and V.A. Evtikhin, Fusion Eng. Des. **81**, 113 (2006).
- [3] G.Z. Zuo *et al.*, Fusion Eng. Des. **89**, 2845 (2014).
- [4] R.B. Gomes *et al.*, Fusion Eng. Des. **83**, 102 (2008).
- [5] F.A. Hernández and P. Pereslavtsev, Fusion Eng. Des. **137**, 243 (2018).
- [6] E. Pickering *et al.*, Entropy **23**, 98 (2021).
- [7] P.C. Stangeby, *The Plasma Boundary of Magnetic Fusion Devices* (IOP Publishing, Bristol, 2000).
- [8] N. Somboonkittichai, J. Phys.: Conf. Ser. **2145**, 012022 (2021).
- [9] J.P. Holman, *Heat Transfer* (McGraw-Hill, Inc., New York, 1981).
- [10] A. Chamber, *Modern Vacuum Physics* (CRC Press, Florida, 2005).
- [11] Y. Jaluria and K.E. Torrance, *Computational Heat Transfer* (Taylor & Francis, New York, 2003).
- [12] W.H. Press *et al.*, *Numerical Recipes: The Art of Scientific Computing* (Cambridge University Press, New York, 2007).
- [13] W.M. Hayes *et al.*, *CRC Handbook of Chemistry and Physics* (CRC Press, Florida, 2014).
- [14] N. Somboonkittichai, Manuscript in preparation (2022).
- [15] Python Software Foundation, *Python 3.8.10 documentation* (Available at <https://docs.python.org/release/3.8.10/>).
- [16] C.R. Harris *et al.*, Nature **585**, 357 (2020).
- [17] P. Virtanen *et al.*, Nature Methods **17**(3), 261 (2020).
- [18] J.D. Hunter, Comput. Sci. Eng. **9**(3), 90 (2007).